# VICTORIA UNIVERSITY
## MELBOURNE AUSTRALIA

*Parametric analysis of pyrolysis process on the product yields in a bubbling fluidized bed reactor*

This is the Accepted version of the following publication

# Parametric Analysis of Pyrolysis Process on the Product Yields in a Bubbling Fluidized Bed Reactor

Salman Jalalifar [a], Rouzbeh Abbassi [b*], Vikram Garaniya [a], Kelly Hawboldt [c], Mohammadmahdi Ghiji [d]

[a] Australian Maritime College, National Centre for Maritime Engineering and Hydrodynamics, University of Tasmania, Launceston, Tasmania, Australia.

[b] School of Engineering, Faculty of Science and Engineering, Macquarie University, Sydney, NSW, Asutralia

[c] Faculty of Engineering and Applied Science, Memorial University, St. John's, NL, Canada.

[d] Institute of Sustainable Industries and Liveable Cities, Victoria University, Victoria, Australia

*Corresponding author, Rouzbeh.abbassi@mq.edu.au

## Abstract

This paper presents a numerical study of operating factors on the product yields of a fast pyrolysis process in a 2-D standard lab-scale bubbling fluidized bed reactor. In a fast pyrolysis process, oxygen-free thermal decomposition of biomass occurs to produce solid biochar, condensable vapours and non-condensable gases. This process also involves complex transport phenomena and therefore the Euler-Euler approach with a multi-fluid model is applied. The eleven species taking part in the process are grouped into a solid reacting phase, condensable/non-condensable phase, and non-reacting solid phase (the heat carrier). The biomass decomposition is simplified to ten reaction mechanisms based on the thermal decomposition of lignocellulosic biomass. For coupling of multi-fluid model and reaction rates, the time-splitting method is used. The developed model is validated first using available experimental data and is then employed to conduct the parametric study. Based on the simulation results, the impact of different operating factors on the product yields are presented. The results for operating temperature (both sidewall and carrier gas temperature) show that the optimum temperature for the production of bio-oil is in the range of 500-525°C. The higher the nitrogen velocity, the lower the residence time and less chance for the secondary crack of condensable vapours to non-condensable gases and consequently higher bio-oil yield. Similarly, when the height of the biomass injector was raised, the yields of condensable increased and non-condensable decreased due to the lower residence time of biomass. Biomass flow rate of 1.3 kg/h can produce favourable results. When larger biomass particle sizes are used, the intraparticle temperature gradient increases and leads to more accumulated unreacted biomass inside the reactor and the products' yield decreases accordingly. The simulation indicated that the larger sand particles accompanied by higher carrier gas velocity are favourable for bio-oil production. Providing a net heat equivalent of 6.52 watts to the virgin biomass prior to entering the reactor bed leads to 7.5 % higher bio-oil yields whereas other products' yields stay steady. Results from different feedstock material show that the sum of cellulose and hemicellulose content is favourable for the production of bio-oil whereas the biochar yield is directly related to the lignin content.

**Keywords:** Biomass, fast pyrolysis, bubbling fluidized bed reactor, Euler-Euler approach, multi-fluid model, bio-oil

### List of symbols

| | |
|---|---|
| $A_i$ | Arrhenius constant, $s^{-1}$ |
| $C_p$ | Heat capacity, J/kg K |
| $d_s$ | Particle diameter, m |

| | |
|---|---|
| $Ea_i$ | The activation energy of reaction $i$, J/mole |
| g | Gravity acceleration, m/s$^2$ |
| $\Delta h$ | Heat release, kJ/kg |
| k | Thermal conductivity, J/kg K |
| $k_i$ | Arrhenius rate constant of reaction $i$, dimensionless |
| MW | Molecular weight, kg/kmole |
| R | Gas constant, J/mole K |
| T | Temperature, Kelvin |
| $U_{mf}$ | Minimum fluidization velocity, m/s |
| Y | Mass fraction |

**Greek symbols**

| | |
|---|---|
| $\alpha$ | The initial mass composition of cellulose in the feedstock, dimensionless |
| $\beta$ | The initial mass composition of hemicellulose in the feedstock, dimensionless |
| $\gamma$ | The initial mass composition of lignin in the feedstock, dimensionless |
| $\rho$ | Density, kg/m$^3$ |
| $\mu$ | Dynamic viscosity, kg/m.s |
| $\eta$ | Product yield |
| $\varepsilon_i$ | Volume fraction of phase $i$, dimensionless |
| $\varepsilon_{mf}$ | Minimum gas volume fraction, dimensionless |

# 1. Introduction

Environmental issues and the unsustainability of fossil fuels has motivated many researchers to seek alternative energy sources [1, 2]. Biomass can be used as a sustainable and eco-friendly source of energy due to its abundance and formation process [3]. All organic material such as agricultural products and its waste, forest residue, land and aquatic animals can be classified as biomass [4-6]. Lignocellulosic biomass contains high energy organics in the form of cellulose, hemicellulose, and lignin which are available in agricultural waste, forest and harvesting crop residues such as corn stover, switchgrass, bagasse etc. [7, 8]. Extracted energy from biomass is greener and more sustainable in comparison to conventional fossil fuels since it has lower emissions of sulfur dioxides ($SO_2$) and particulate matter (PM) [9]. Carbon neutrality is another benefit of biomass which means that due to the life cycle of biomass, the photosynthesis process is able to recycle the released carbon dioxide ($CO_2$) into the environment [9, 10]. Conversion of biomass to an upgraded quality fuel such as a liquid or more homogenous solid is also achievable [11, 12]. The possible routes are thermochemical conversions which are mainly; provision of heat via direct combustion, a synthesis gas generation by gasification; production of bio-oil, char, and non-condensable gas through pyrolysis process [10]. The generated products of biomass pyrolysis are beneficial for some applications including bio-oil for liquid fuel as a source of high-value chemicals; solid biochar (e.g. sustainable source for adsorbent, soil amendment, or catalyst); and biogas for energy recovery [13, 14]. Pyrolysis is categorized into three different groups; slow, fast, and flash pyrolysis. Char is the primary product of slow pyrolysis whereas the primary product of fast and flash pyrolysis is the liquid bio-oil. The produced bio-oil can be used for co-generation of heat and power in boilers, gas turbines, and diesel engines, or it can be upgraded to a higher quality fuel after refining [15-17].

In recent years, numerous experimental [3, 18-23] and numerical [24-35] studies have investigated the biomass pyrolysis process. Although performing an experimental test is inevitable for finalizing the design and optimization of the pyrolysis process, it is very costly and time-consuming. In addition, a detailed understanding of complex physical phenomena such as multiphase flow dynamics, heat and mass transfers, and chemical kinetics that take place simultaneously inside the reactors, is challenging. Computational Fluid

Dynamic (CFD) modelling techniques can be used as a tool in a better understanding of these types of systems. Moreover, CFD can model the internal temperature and pressure changes that are hard to measure in the harsh conditions of the reactor environment. CFD simulations can provide an insight into transport phenomena by giving an indication of the product yields of the pyrolysis process in reactors. In CFD simulations different reaction mechanisms can be exchanged in and out depending on feedstock and pyrolysis conditions/reactors. The heterogeneity of the biomass and the multiphase flow make the reaction mechanism complex, however global reaction rates have been proposed by various researchers e.g. [30, 31]. Typically, global reactions are assumed where the biomass is converted through a series of primary and secondary reactions [36]. The reaction rates are typically derived in reactors where heat and mass transfer resistances are minimized. To properly model a pilot or commercial scale reactor, these resistances must be included in the form of transport equations.

Widespread applications of fluidized bed reactors (FBR) have prompted the use of CFD simulations as a tool in design [27-34, 37-41], to investigate impacts such as nitrogen and sidewall temperature, sand particle size, biomass feed rate and particle size, feedstock material, residence time and nitrogen velocity. The amount of extracted bio-oil from pyrolysis of biomass is determined by feedstock, operating temperature, and residence time of the condensable vapours [42]. At higher temperatures and longer vapour residence time, the possibility of secondary cracking reactions increased leading to lower yields of non-condensables and higher water content. There are some techniques to vary the residence times in fluidized beds such as the variation of carrier gas velocity and the location of the biomass feed injector relative to the reactor height [38]. The biomass feed rate is a factor in solid particle residence time. There is a balance between minimizing secondary reactions and ensuring the biomass particles are well mixed and reach thermal equilibrium [35]. To enhance heat transfer between hot sand and cold biomass particles, they need to be blended together. Hence, the nitrogen velocity must exceed the minimum fluidization velocity in order to maximize the mixing of solid particles. However, too high nitrogen velocity causes sand carryover from the reactor. The biomass particle size determines the heating rate of the particle and ideally fine particles are used to minimize intraparticle heat and mass transfer resistances. However, there is a balance between minimum particle size and costs to grind to this size [43]. Table 1 illustrates some other studies and discusses the application of CFD and their major findings in reacting multiphase flow.

There are a number of CFD software packages capable of modeling reacting multiphase flow dynamics in different types of reactors and processes. For instance, ANSYS FLUENT [25, 44, 47, 52-54], Multiphase Flow with Interphase eXchanges (MFIX) [33, 37, 55, 56], OpenFOAM [26, 27, 29, 30, 35, 38, 57, 58] etc. have been used frequently for simulation of reacting multiphase flow including combustion [52], gasification [52-54] and pyrolysis process [44, 47, 48, 52, 56, 59]. Among them, ANSYS FLUENT has attracted the attention of engineers and researchers due to features including its user-friendly environment, capability of modelling complex geometries inside ANSYS workbench interface, programming facility by adding user defined functions (UDF), having most recent empirical correlations for granular heat transfer and drag as well as the KTFG (Kinetic Theory of Granular Flow); models that are needed for description of interphase transport phenomena. Therefore, ANSYS Fluent is an appropriate tool for numerical simulations of reacting multiphase flow for different reactor types with complex geometries from lab-scale and pilot scale to industrial scale.

In this paper, a CFD model is implemented to study a 2-D standard lab-scale bubbling fluidized bed reactor (BFBR). The model is validated first based on the available experimental data. A parametric study has then been conducted to address the effect of the most important influential parameters on the product yields of the process. In addition to the aforementioned parameters, the present paper investigates the effect of the intraparticle temperature gradient, biomass preheat and different feedstock material (seven feedstocks) on product yields. A wide range of biomass feed rate is analysed so that the effect from this parameter, on the product yields, can be more thoroughly assessed. This can assist in identifying an optimal setting with more efficient energy consumption. The possible methods for achieving the optimum amount of desired yields are proposed.

**Table 1.**

CFD studies of typical reacting multiphase flow

| Author(s) | Reactor type | Process type | Dimension | Major findings |
|---|---|---|---|---|
| Cardoso et al. [25] | BFBR | Gasification | 2-D | • Tendency of biomass particles is to be in the middle and upper regions of the bed whereas sand particles accumulate at the middle and bottom of the bed.<br>• Lighter biomass particles move towards the top of the bed, and heavier biomass particles mixed with the sand particles.<br>• Increased superficial gas velocity improved the binary mixing.<br>• Biomass particles move upwards across the bed at the reactor's centreline and downwards in the near-wall region.<br>• Smaller biomass particles allowed for a better heat transfer. |
| Eri et al. [44] | BFBR | Fast pyrolysis | 2-D | • Cellulose-rich biomass produces more bio-oil than other biomass types.<br>• The content of lignin has a close relationship with char production. |
| Kulkami et al. [45] | Vortex reactor | Fast pyrolysis | 3-D | • Segregation of unwanted char particles towards the exhaust leads to lower undesirable gas-char contact, which resulted in more convective heat transfer coefficient between gas-solid and eventually higher yield of bio-oil. |
| Peng et al. [46] | BFBR | Fast pyrolysis | 2-D | • The product yields and reaction rates are a strong function of pyrolysis temperature<br>• Cellulose had the strongest ability to produce bio-oil, while lignin had the strongest ability to produce char. |
| Zhong et al. [47] | BFBR | Fast pyrolysis | 2-D | • The particle shrinkage effect is applied to the complex pyrolysis mechanism.<br>• The scheme has little impact on volume fraction and temperature distribution but influential impact on velocity distribution, mass fraction, diameter, and density, which finally effects the product yields. |
| Lathouwers and Bellan [48, 49] | FBR | Fast pyrolysis | 2-D | • The most influential factor on the bio-oil yield is the operating temperature. |
| Aramideh et al. [50, 51] | Auger reactor | Fast pyrolysis | 3-D | • The optimal wall temperature for maximum bio-oil production is about 823 K.<br>• Increased pre-treatment temperature of biomass led to lower bio-oil yield.<br>• Higher nitrogen flow rate resulted in higher bio-oil whereas increased biomass feed rate led to lower bio-oil yield. |

# 2. Methodology

In this paper, multi-phase fluid dynamics is taken into account by using conservation laws of mass, momentum, energy, and species in Eulerian-Granular approach. To simulate biomass fast pyrolysis, a combination of Multi-Fluid Model (MFM) and a chemical solver is essential. Description of MFM model and chemical kinetics are as follows.

## 2.1. Multi-fluid model

In the MFM, all phases are treated as inter-penetrating continua. Typically, MFM consist of one gas phase (primary phase) and an arbitrary number of solid phases (secondary phases). In this study, as shown in Fig.1, each phase consists of different species; three species for gas phase (condensable vapours, non-condensable gases, and nitrogen), seven species for biomass phase (virgin cellulose, virgin hemicellulose, virgin lignin, active cellulose, active hemicellulose, active lignin, and biochar), and one species for sand phase. Thus, eleven species are involved in the process. By considering the volume fraction of each phase, the conservation equations for each phase are derived separately. In addition to the fundamental conservation equations, some extra equations such as stress-strain tensor for momentum equations, conductive heat flux for energy equations, and diffusive flux for species equations are needed. However, in the derivation of the equations, some unknown

terms are produced which necessitates using closure models. In the interaction of gas-solid phases, two models are proposed. The first model is the empirical correlations (drag and heat transfer correlations) which is required for interphase transport correlations and the second is the Kinetic Theory of Granular Flow (KTFG) [60], which is needed for calculation of granular temperature, pressure, viscosity, etc. Detailed description of the models can be found in the literature [29, 33, 35, 37].
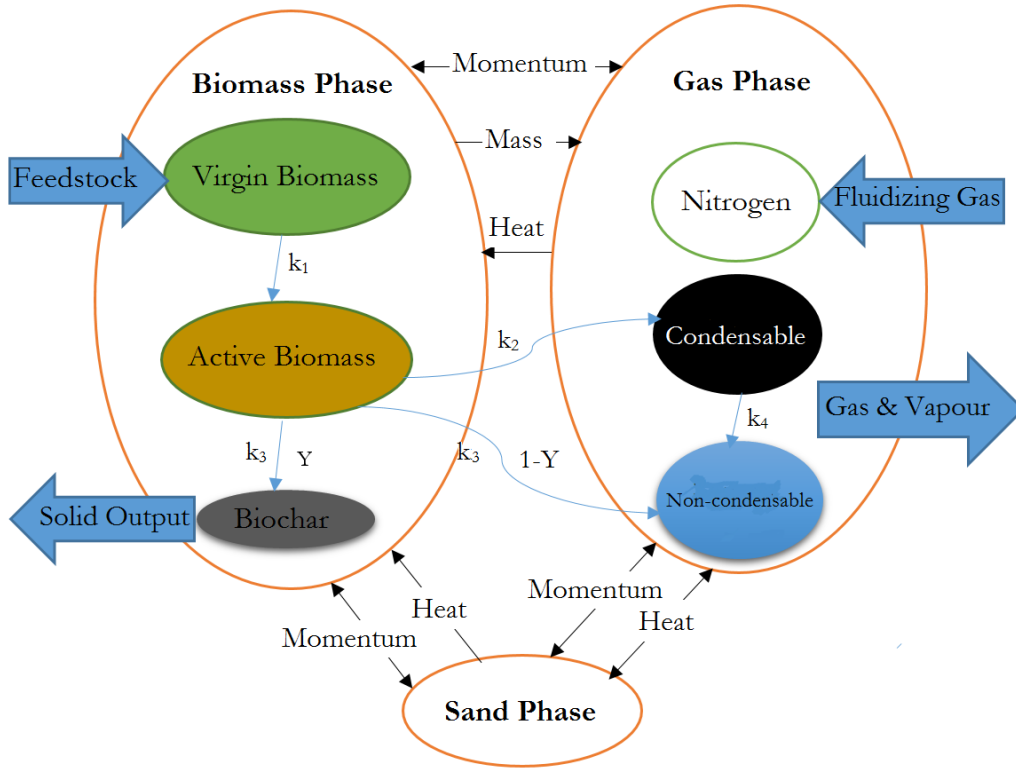


**Fig. 1.** Chemical reactions and exchange of mass, momentum, and heat between phases.

## 2.2. Chemical kinetics of a single biomass particle

Since many elementary reactions are involved in the biomass pyrolysis process [61], lack of knowledge about the actual chemical reactions and compounds formed for the specific biomass makes development of a detailed and fundamental decomposition mechanism difficult [62]. In order to capture the devolatilization of the biomass and secondary cracking, a lumped global kinetics was used. A single-component single-step reaction kinetics was first proposed by Shafizadeh and Chin [63] to describe the wood thermal decomposition. However, the proposed method was not able to predict the secondary cracking caused by depolymerization [64]. Further, it is proposed that the biomass is initially devolatilized to reach an intermediate stage, or activated biomass [65]. These shortcomings are addressed using single-component multistep reaction kinetics proposed by Shafizadeh and Chin [63]. Subsequently multicomponent single-step reaction kinetics was considered to individually account for the effect of each biomass component (cellulose, hemicellulose and lignin) [66]. Eventually, multicomponent, multistep reaction kinetics have been proposed by Ward and Braslaw [67], Koufopanos et al. [68, 69], Orfao et al.[70], Miller and Bellan [71]. It is proposed that multicomponent multistep reaction kinetics is the most accurate and feasible method for practical application [72]. Although using the lumped reaction schemes is straightforward, the predictability of the product yields using numerical simulations is strongly dependent on the accuracy of the reaction kinetics. Thus, in recent years, some research has been performed considering comprehensive and relatively complex reaction kinetics [73, 74].

In this study, a superimposed reaction kinetics based on multicomponent multistep reaction kinetics is used to simulate the fast pyrolysis of the biomass. As mentioned, the feedstock material is considered a lignocellulosic biomass, which can be stated as:

$$\text{Biomass} = \alpha \text{Cellulose} + \beta \text{Hemicellulose} + \gamma \text{Lignin} \qquad (1)$$

Where ($\alpha, \beta, \gamma$) is the initial mass composition of biomass. The rate of pyrolysis is the sum of each component's rate so that the contribution of each component is proportional to its mass fraction. In the kinetic model, virgin biomass converts to "active material" which then reacts to condensable, non-condensable and char. Subsequently in the secondary reaction, condensable reacts to form non-condensable. As illustrated in Fig. 1, three different phases including biomass phase, sand phase and gas phase are taken into account. Each phase involved in the process has a number of species. The biomass phase includes virgin and active biomass and char while the gas phase includes condensable, non-condensable and nitrogen. The sand phase and nitrogen are inert and do not participate in the chemical reactions. The reaction rate constants are calculated as below:

$$k_i = A_i \exp\left(-\frac{Ea_i}{RT}\right) \qquad (2)$$

where $k_i$ is the rate constant for reaction "$i$", and $A_i$ and $Ea_i$ are the associated Arrhenius constant and activation energies. "$T$" is the temperature in Kelvin and "$R$" is the gas constant. As indicated previously, overall, eleven different species are included in this reaction scheme; the solid reaction phase (virgin biomass, active biomass and biochar), the condensable/non-condensable phase, and the non-reacting sand phase. The nitrogen is included in the gas phase as it contributes to partial pressures but does not react. The values of the kinetic parameters for the reaction scheme and the obtained values for heat of reaction are outlined in Table 2. Y is the formation ratio for the char component, which is 0.35, 0.6, and 0.75 for pyrolysis of cellulose, hemicellulose, and lignin, respectively [37]. The thermo-physical properties of species involved in the reactions of the biomass are given in Table 3. It is worth noting that the incompressible ideal gas model calculates the density of gaseous species and the viscosity of the solid species are calculated based on the granular models.

**Table 2**
Pre-exponential factors and activation energies for the biomass component [37].

| Components | Reaction | A($s^{-1}$) | E(MJ/kmole) | Heat release, $\Delta h$ (MJ/kmole) |
|---|---|---|---|---|
| Cellulose | $k_{1C}$ | $2.8 \times 10^{19}$ | 242.4 | 0 |
| | $k_{2C}$ | $3.28 \times 10^{14}$ | 196.5 | 41.35 |
| | $k_{3C}$ | $1.3 \times 10^{10}$ | 150.5 | -3.24 |
| Hemicellulose | $k_{1H}$ | $2.1 \times 10^{16}$ | 186.7 | 0 |
| | $k_{2H}$ | $8.75 \times 10^{15}$ | 202.4 | 33.69 |
| | $k_{3H}$ | $2.6 \times 10^{11}$ | 145.7 | -2.64 |
| Lignin | $k_{1L}$ | $9.6 \times 10^{8}$ | 107.6 | 0 |
| | $k_{2L}$ | $1.5 \times 10^{9}$ | 143.8 | 53.09 |
| | $k_{3L}$ | $7.7 \times 10^{6}$ | 111.4 | -4.16 |
| Tar | $k_4$ | $4.25 \times 10^{6}$ | 108.0 | -4.2 |

**Table 3**
Thermo-physical properties of species [49].

| Species | Density $\rho$ (kg/m³) | Particle diameter $d_s$ (m) | Molecular weight (g/mol) | Heat capacity $C_p$ (J/kg K) | Dynamic viscosity $\mu$ (kg/ms) | Thermal conductivity k (J/kg K) |
|---|---|---|---|---|---|---|
| Condensable | - | - | 100 | 2500 | $3\times10^{-5}$ | $2.577\times10^{-2}$ |
| Non-condensable | - | - | 30 | 1100 | $3\times10^{-5}$ | $2.577\times10^{-2}$ |
| $N_2$ | - | - | 28 | 1121 | $3.58\times10^{-5}$ | $5.63\times10^{-2}$ |
| Biomass | 400 | $4\times10^{-4}$ | * | 2300 | - | 0.3 |
| Biochar | 2333 | $4\times10^{-4}$ | 12.01 | 1100 | - | 0.1 |
| Sand | 2649 | $5.2\times10^{-4}$ | 60.08 | 800 | - | 0.27 |

*Molecular weight of the biomass components are 162.14, 132.11, and 208.21 (g/mol) for cellulose, hemicellulose, and lignin, respectively.

# 3. Experimental validation

To validate the numerical simulations, a standard lab-scale bubbling fluidized bed reactor based on the experimental study of [33] is used. The 2-D computational domain is shown in Fig. 2. Biomass with a diameter of 0.4 mm at an inlet temperature of 300 K is fed at a rate of 100 g/h. Nitrogen flows from the bottom of the bed at a velocity of 0.36 m/s and temperature of 773 K. The sand with a diameter of 0.52 mm is initially packed to a height of 5.5 cm with a volume fraction of 0.59. The outflow boundary condition is used at the outlet. No-slip wall condition is applied to the solid walls. To simulate external heating, the wall temperature is kept constant at 800 K up to a height of 8 cm. The bed temperature is initially set to 773 K. The biomass feedstock is red oak with a composition of $(\alpha, \beta, \gamma) = (0.41, 0.32, 0.27)$. A grid independency study is carried out using 2-D mesh with four different grid resolutions for pure cellulose as a feedstock. The number of meshes for cases 1-4 are 225, 910, 2055, and 3640, respectively. The centreline temperature distribution of the reactor is shown in Fig. 3. Since there is no significant difference between cases 3 and 4, to save computational costs, case 3 with 2055 meshes is selected for further simulations. At the beginning of the simulations, small time step size of $1\times10^{-4}$ s is used to avoid numerical instability. However, the adopted grid resolution allows us to increase the time step size to $5\times10^{-4}$ s without any numerical instability. In the species transport equations, the mass fraction of each species must sum to unity. Therefore, the $N_{th}$ mass fraction is determined as one minus the sum of the N-1 solved mass fractions. To reduce the numerical error, the $N_{th}$ species should be selected as the species with the overall largest mass fraction (nitrogen in the gas phase and cellulose in the biomass phase).

For the numerical simulations, FLUENT solver V18.0 is used. The Eulerian-Granular approach is taken into account for the solution of laminar multiphase flow by activating both the energy and species transport equations. The conservation equations are solved in two fractional steps. In the first fractional step, reaction terms set to zero considering only the spatial solution of the multiphase species. In the second fractional step, a stiff ODE (Ordinary Differential Equations) solver is employed by integrating the reactions terms in each cell. The second-order implicit method is used for time discretization. The least square cell-based is applied to the pressure-based solver and phase coupled SIMPLE-algorithm for the pressure-velocity coupling. Momentum, energy and species equations are discretized by the second order (upwind) method. The volume fraction is calculated using the QUICK algorithm. Finally, each phase, especially the sand phase, is initialized by hybrid initialization; and are patched based on the initial packing limit.
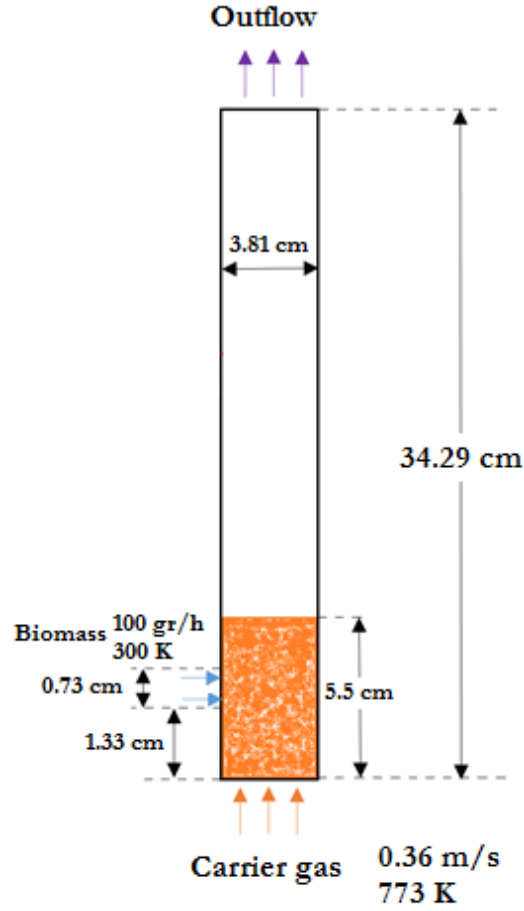
**Fig. 2.** Schematic geometry of 2-D model of bubbling fluidized bed for simulations.
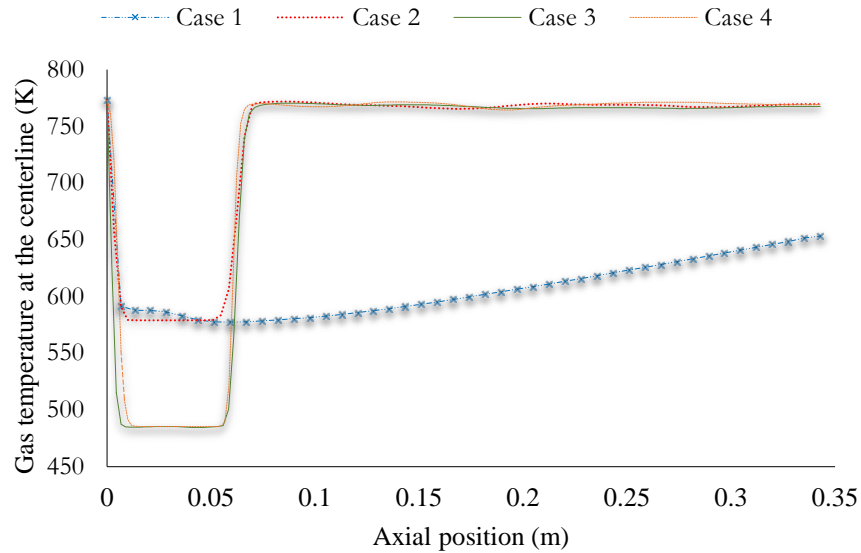


**Fig. 3.** Axial distribution of gas temperature at statistically steady state condition using different grid sizes. case 1: 225 meshes, case 2: 910 meshes, case 3: 2055 meshes, and case 4: 3640.

The product yields are calculated by integrating across the reactor outlet. For example, the condensable yield is calculated as follows:

$$\eta_{Condensable} = \left\{ \int_{t_{sss}}^{t_{sss}+\Delta t} \int_{outlet} (\varepsilon_g \rho_g U_g Y_{condensable}) dAdt \right.$$

$$\left. / \int_{t_{sss}}^{t_{sss}+\Delta t} \int_{outlet} [\varepsilon_g \rho_g U_g (Y_{condensable} + Y_{non-condensable}) + \varepsilon_{biomass} \rho_{biomass} U_{biomass} (Y_{biochar} + Y_{unreacted-biomass}) dAdt \right\} \quad (3)$$

where $t_{sss}$ is the time for reaching statistically steady state condition, $\Delta t$ is the last 20 seconds of the simulation physical time after reaching statistically steady state condition. $\varepsilon$, $\rho$, $U$ is the volume fraction, density, and velocity of each phase, respectively. Index $g$ in equation 3 represent the gas phase. Y is the mass fraction of each species in the specified phase. The comparison of product yield for pyrolysis of red oak as a feedstock material against experimental data [33] is shown in Table 4.

**Table 4**
Comparison of product yield for red oak pyrolysis (wt %) between simulation and experiment

| Components | Condensable | Non-condensable | Biochar | Unreacted biomass | Temperature (°C) |
|---|---|---|---|---|---|
| Experiment [33] | 71.7±1.4 | 20.5±1.3 | 13±1.5 | - | 500 |
| Current study | 62.4 | 16.9 | 11.2 | 9.5 | 493 |

The predicted results for biochar show a good agreement with the published experimental data. The results obtained for condensable vapours are comparable to the experimental ones. However, the results for non-condensable gases under predicted the experimental values. The difference between the numerical and experimental bed reactor temperature is due to heat transfer from hot sands, heated wall and hot carrier gas to cold virgin biomass. The percentage of discrepancy between the experiment and the simulation results for condensable, non-condensable, biochar, and operating temperature are 13, 17.6, 13.8, and 1.4 , respectively

# 4. Results and discussion

In this section, the results for biomass fast pyrolysis in the bubbling fluidized bed reactor illustrated in Fig. 2 are presented. The common method for calculation of the product yields, used by researchers [27, 29, 33, 35, 37, 38] monitors the product outflux at the reactor outlet. Since many fluctuations are witnessed in the outflux of the product in the reactor outlet, the decision about the time of achieving the statistically steady state condition (a state in which the mean field of variables are the object of interest despite the fluctuations in some flow properties) is challenging. It should be noted that statistically steady state condition for the simulation results occurs at a different physical time for different parameters. Thus, the criteria for deciding whether the steady state condition is obtained or not is carried out by taking into account the temperature outlet and outflux of products (condensable, non-condensable, and biochar).

## 4.1. Effect of biomass feed rate

Fig. 4. shows the effect of biomass feed rate on the product yields. It can be seen that below 1.3 kg/h the product yields are relatively constant. This implies that when the biomass feed rate is not too high, the biomass contact with heated wall and mixing with hot sand, and hot carrier gas, results in high heat transfer and possible lower fluctuations in temperature therefore reaction rates are not affected by the feed rates. These findings are comparable with other published results [35, 49]. However, by introducing more mass flux (>1.3 kg/h), the supplied heat is insufficient for biomass particles to reach the operating temperature of the reactor. The small increase in biochar is not significant whereas the large increase in unreacted biomass is significant which resulted in lower production of condensable vapours and non-condensable gases. This range of feed rates was

used to find an optimal energy consumption, which in this case is 1.3 kg/h. We need to find how far we can increase the feed rates to prevent waste of energy.
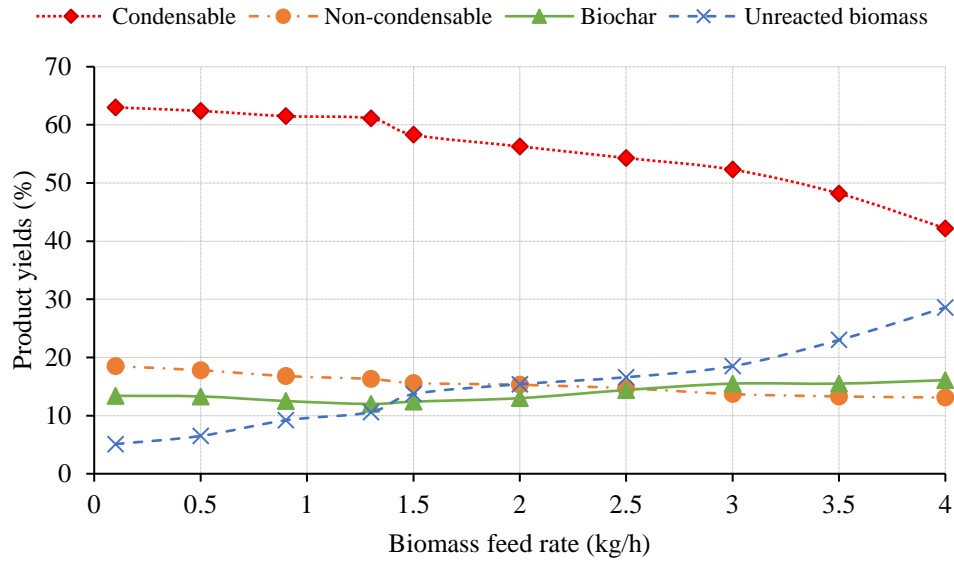


**Fig. 4.** Product yields' variation with respect to biomass feed rate

## 4.2. Effect of biomass particle size

In Fig. 5, the effect of biomass particle size on the product yields is shown. Contrary to other published results [35], in this study, the effect of the intraparticle temperature gradient is considered. It is noteworthy that for larger particles the intraparticle temperature gradient plays an important role in the product yields as the larger particles show a higher unreacted biomass fraction. However, it should be noted that with respect to the reacted biomass, the particle size does not play a role in the ratios of the different products (i.e. 0.66, 0.2, 0.14 for condensable, non-condensable, and biochar, respectively). There is no limit for the size of large particles used. As long as the provided heat is sufficient, larger biomass particles can be used if they are surrounded by sand particles of suitable sizes to maximize heat transfer from hot sand particles to cold virgin biomass particles. However, it is more efficient to have smaller biomass particles since the intraparticle temperature gradient is lower for smaller particles. Therefore, despite the increased costs, grinding biomass particles are inevitable. On the other hand, if the biomass particles are too tiny, unreacted particles may be thrown out of the reactor bed by the carrier gas. In conclusion, deciding on an optimal size for biomass particles depends on many different factors and cannot be determined with certainty.
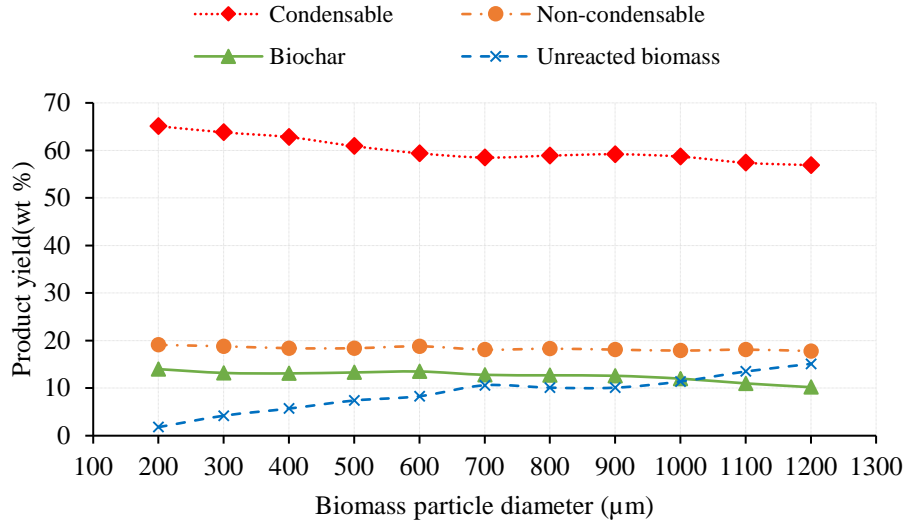
**Fig. 5.** Product yields variation with respect to biomass particle size

## 4.3. Effect of sand particle size

For specific nitrogen velocity, the bed expansion is lower for larger sand particles. In other words, the larger the sand particle size the less efficient is the fluidization. When larger sand particles are used, the minimum fluidization velocity rises and necessitates higher carrier gas velocity in order for the particles to fluidize. The minimum fluidization velocity [35] is;

$$U_{mf} = \frac{d_s^2}{150\mu_g} g(\rho_s - \rho_g)\frac{\varepsilon_{mf}^3}{1-\varepsilon_{mf}} \tag{4}$$

where $d_s$ is the mean sand particle diameter, $\varepsilon_{mf}$ is the minimum gas volume fraction, $g$ is the gravity acceleration, $\rho_s$ and $\rho_g$ are the density of solid and gas phases, respectively. Table 5 illustrates the variation of minimum fluidization velocity with respect to sand particle's diameter.

**Table 5**
Minimum required nitrogen velocity for effective fluidization.

| Minimum fluidization velocity (m/s) | Sand particle size ($\mu m$) | Nitrogen velocity |
|---|---|---|
| 0.08 | 400 | 0.2 |
| 0.13 | 500 | 0.3 |
| 0.19 | 600 | 0.4 |
| 0.25 | 700 | 0.5 |
| 0.33 | 800 | 0.6 |
| 0.42 | 900 | 0.7 |
| 0.52 | 1000 | 0.8 |

The predicted product yields with respect to sand particle's diameter are shown in Fig. 6. As it can be seen, the trend is similar to the effect of nitrogen velocity (Fig. 8). By increasing the sand particle size, the required carrier gas velocity for effective fluidization rises, and consequently the residence time decreases which minimizes secondary cracking of condensable vapours to non-condensable gases. Moreover, when biomass particles are surrounded by larger sand particles, appropriate heat transfer from hot sand particles to cold virgin

biomass particles rises due to higher heat transfer area. This phenomenon results in lower biochar yield and unreacted biomass. These results are consistent with other researchers findings [35].

Hot sand particles plays the role of heat carrier to the biomass particles. Sand particles need to surround the biomass particles effectively in order to facilitate the heat transfer between hot sand particles and cold virgin biomass. Therefore, it will be more efficient if sand particles are larger than biomass particles. This will also increase the heat transfer surface area. The only limit for using larger sand particles is their fluidization. Therefore, the optimal condition that can be decided for sand particle size depends on some factors including biomass particle size and fluidizing gas velocity.
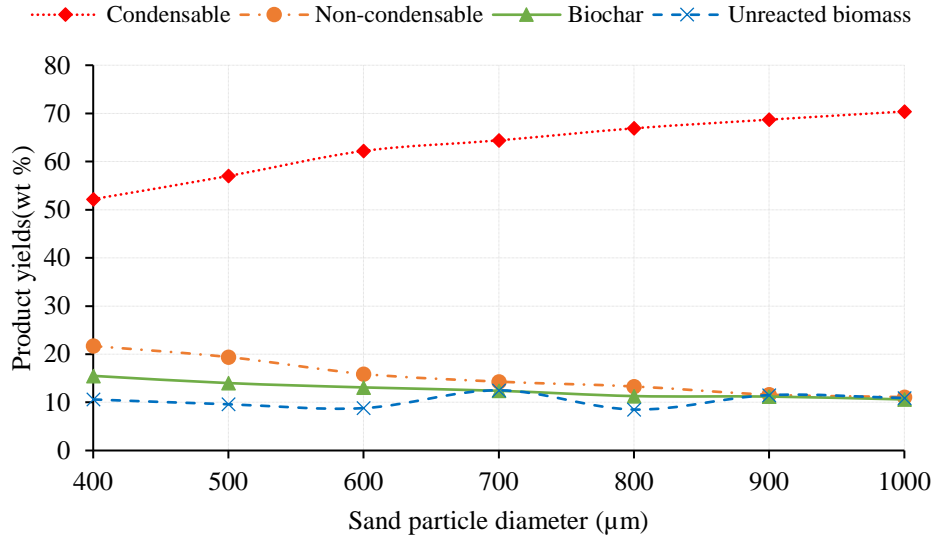


**Fig. 6.** Product yields' variation with respect to sand particle size.

## 4.4. Effect of biomass injector location

As the biomass injector is moved to a higher location, the production of condensable vapours rises and non-condensable gases decreases (Fig. 7). Moving the injector to a higher location decreases the solids and vapour residence time and thereby minimizes cracking of condensable vapours to non-condensable gases. In this case, the rate of secondary crack of condensable vapours to non-condensable gases varies from 0.089 to 0.036 kg/h in the range of 16.5-20 mm of injector height. It is worth noting that the limit for biomass injector location is the maximum packing limit. Otherwise, the higher the position of the injector, the shorter the residence time and the higher the yield of condensable vapours. Therefore, the optimal height for the biomass injector depends on the initial packing limit of the sand particles.
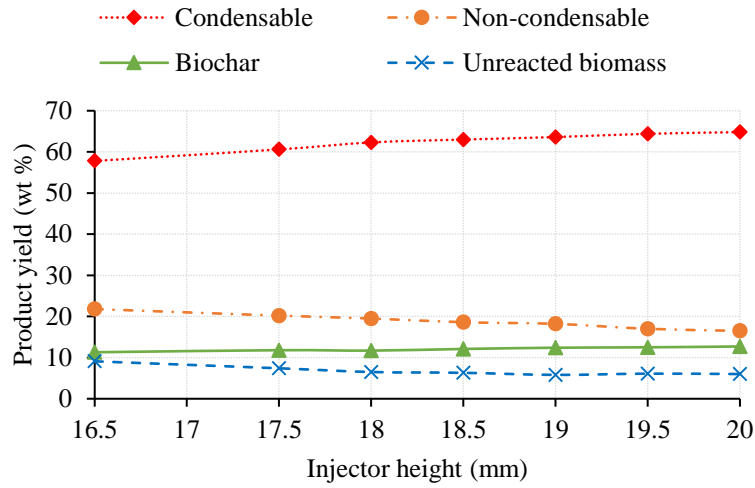
**Fig. 7.** Product yields' variation with respect to biomass injector height.

## 4.5. Effect of nitrogen velocity

The effect of superficial nitrogen velocity on the product yields is shown in Fig. 8. As the carrier gas velocity increases, condensable yields increase, non-condensable and unreacted biomass decrease, whereas the char yields remain constant. The increase in condensable and a decrease in non-condensable values are due to shorter residence time (minimizing secondary cracking reactions). These results are in agreement with previous findings from literature [33, 35, 38]. The lower limits for nitrogen velocity are determined by the minimum fluidization velocity, which depends on the sand particle size (Table 5). However, the carrier gas velocity can be increased to the extent that does not force the unreacted biomass particles and sand particles out of the reactor bed. Therefore, the optimal nitrogen velocity depends primarily on particle sizes.
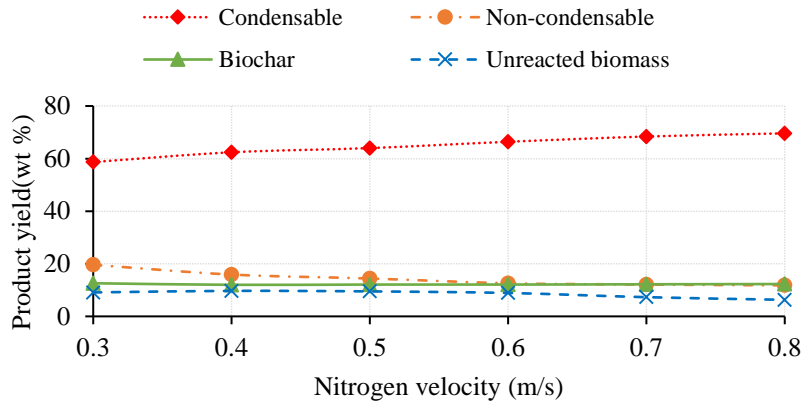


**Fig. 8.** Product yields' variation with respect to carrier gas velocity.

## 4.6. Effect of operating temperature

In Fig. 9 the effects of both sidewall and nitrogen temperature on the product yield are demonstrated. The yield of non-condensable is constantly growing for two possible reasons. Firstly, a rise in the temperature improves devolatilization and increases the reaction rates. Secondly, at higher temperatures, secondary crack occurs which converts condensable vapours to non-condensable gases. For instance, the secondary reaction rate varies

from 0.005 to 0.198 kg/h at a temperature range of 400-675 °C. On the other hand, the yield of condensable initially increases as the devolatilization and reaction rates increase, and then decreases due to the secondary crack, which decomposes condensable vapours to non-condensable gases. These findings are in accordance with a previous study [35]. The maximum bio-oil yields occur in the range of 500-525°C as an operating temperature. However, with further increase in temperature, secondary cracking reactions are favoured and result in a precipitous decrease in condensable yield. In other words, as the temperature exceeds 600°C, the process behavior is more like gasification than fast pyrolysis. Hence, condensable vapours, unreacted biomass and biochar decrease with the increase in temperature. Fast pyrolysis process occurs at moderate temperatures and its optimal temperature is in the range of 500-550 ºC. At higher or lower temperatures other than these values, the condensable yield decreases. Therefore, in this paper a temperature range of 400-675 ºC is considered to see the effect of lower and higher temperatures on all product yields.
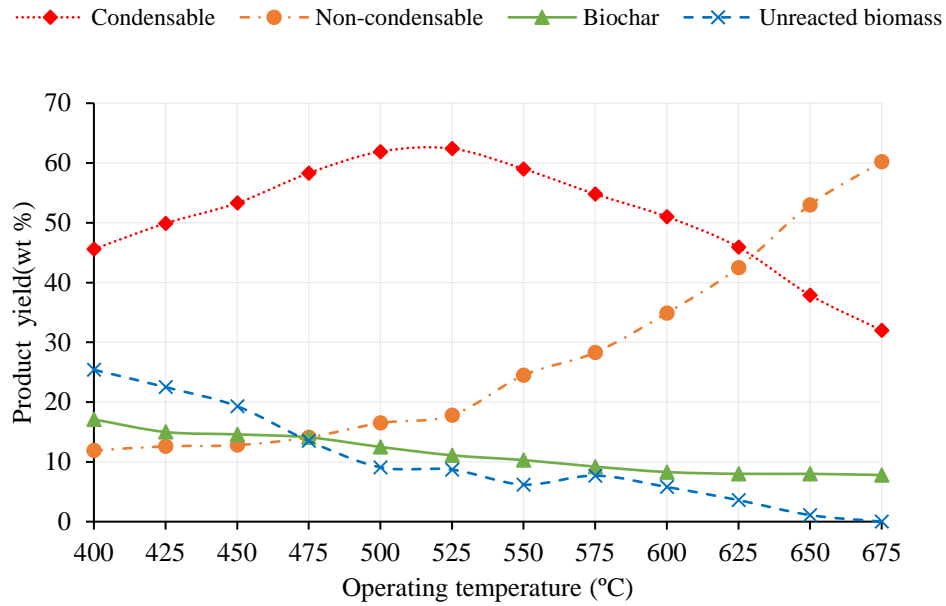


**Fig. 9.** Product yields' variation with respect to carrier gas temperature.

### 4.7. Effect of biomass preheat

The effect of biomass preheat prior to injection inside the reactor is illustrated in Fig. 10. When the biomass is preheated, it reaches the active state more quickly and with a further heat transfer provided by the heated wall, sand, and hot carrier gas, more proportion of biomass is converted to the products. Therefore, unreacted biomass decreases whereas biochar yield remains steady. In addition, more reacted biomass means more production of condensable and non-condensable. Since by preheating the virgin biomass, the active state is reached faster and the residence time is shortened which leads to higher condensable and lower non-condensable yields. Thus, altogether, preheating has a favourable effect on condensable yields whereas non-condensable yields remain stable. It is worth noting that preheating of the virgin biomass from an ambient temperature of 298 K to a temperature of 400 K is equivalent to 6.52 watts of net heat energy. Therefore, it would be more efficient to spend some of the energy on preheating of the biomass prior to reaching the reactor bed provided that no reactions occur outside the reactor bed. The maximum temperature rise that is considered for pre-entry stage is $\Delta T = 100$ K. Therefore, as long as no reaction takes place in the biomass feeder, preheating the biomass will maximize the bio-oil yield.
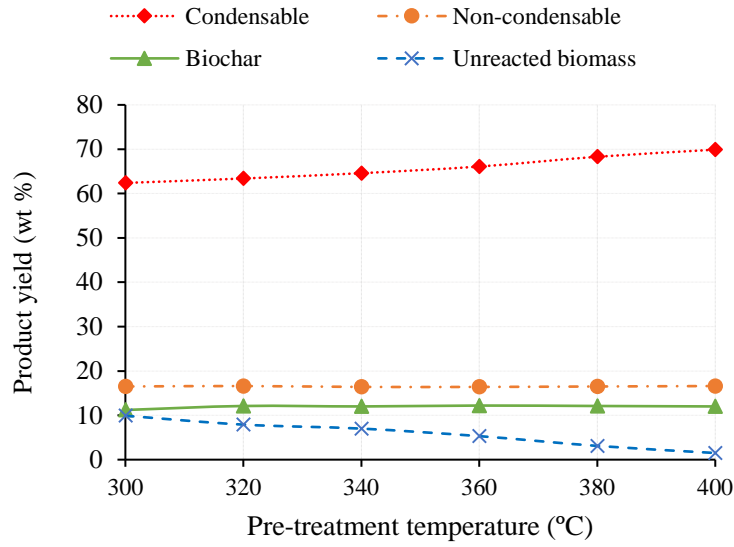
**Fig. 10.** Product yields' variation with respect to pre-treatment temperature.

## 4.8. Effect of feedstock material

Since the model is capable of predicting product yields from different lignocellulosic biomass with different biomass components, seven different feedstocks are taken into account to allow a wide range of feedstock material to be studied. However, any other type of biomass with other contentsuch as water content and impurities is beyond the scope of this paper. Various feedstocks and their components are illustrated in Table 6. Fig. 11 shows the simulation results for different feedstocks. The results show that the sum of cellulose and hemicellulose content of the material is a more favourable component for the bio-oil production whereas the lignin content contributes to more biochar yields. Fig. 12 shows this trend in a different way. The biochar yield linearly changes with lignin content and condensable yield rises when the sum of cellulose and hemicellulose content increases. The most condensable yield is anticipated from pure cellulose whereas the most biochar yield is predicted from olive husk fast pyrolysis.

**Table 6**
The initial mass fraction of biomass $(\alpha, \beta, \gamma)$ in equation (1)

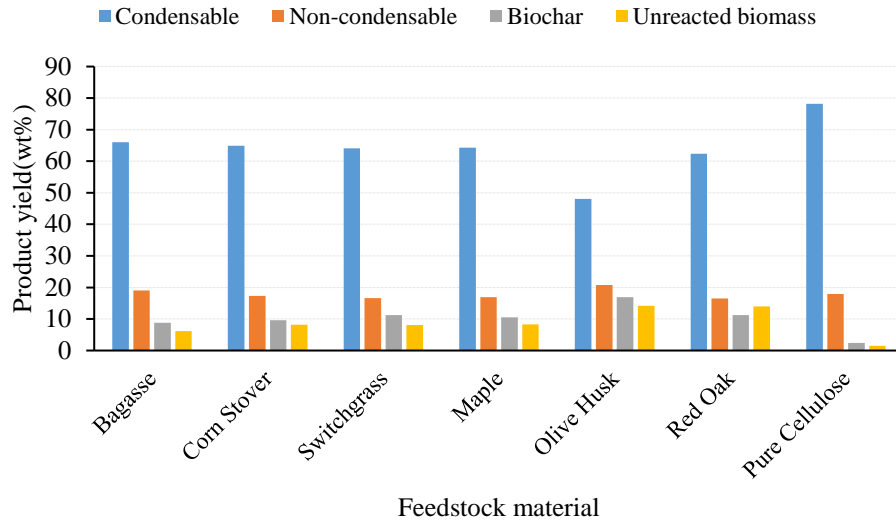| Feedstock | Pure cellulose | Red oak | Bagasse | Corn Stover | Switchgrass | Maple | Olive husk |
|---|---|---|---|---|---|---|---|
| Cellulose | 1 | 0.41 | 0.36 | 0.48 | 0.42 | 0.40 | 0.22 |
| Hemicellulose | 0 | 0.32 | 0.47 | 0.30 | 0.34 | 0.38 | 0.33 |
| Lignin | 0 | 0.27 | 0.17 | 0.22 | 0.24 | 0.22 | 0.45 |

**Fig. 11.** Product yields' variation with respect to different biomass feedstock.
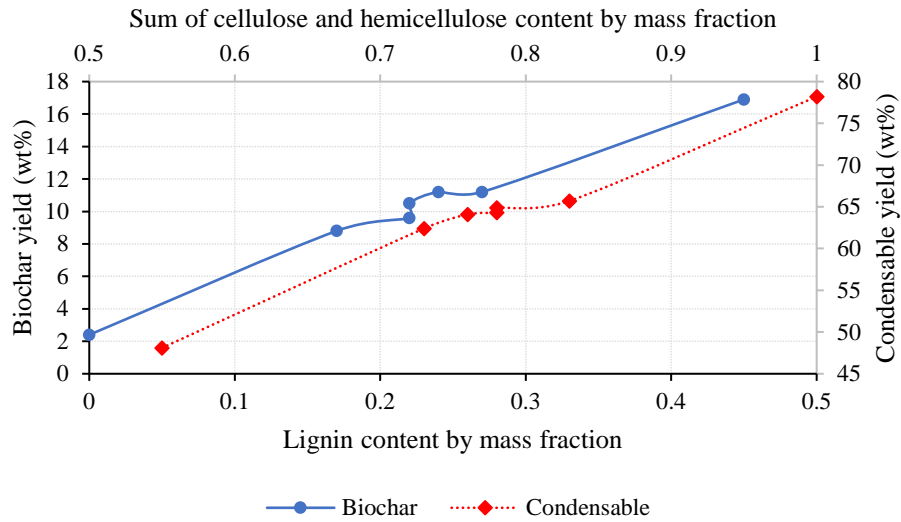


**Fig. 12.** Product yields' variation with respect to the component content of feedstock material

Although in the current paper the authors addressed most of the influential factors in biomass fast pyrolysis in a bubbling fluidized bed reactor, the following factors can also be taken into account for future studies:

- **Initial sand packing limit:** in this study, sand is initially packed to the height of 5.5 cm with porosity of 0.61. The effect of other packing heights can be taken into account.

- **Effect of catalytic particles:** in this paper, two solid phases are considered including solid phase 1 or reacting biomass phase and solid phase 2 or inert sand phase. What happens if the solid phase 2 is catalyst or a mixture of catalyst and non-catalyst particles? In this case, the previous chemical kinetics and reaction rates are not applicable and other chemical kinetics need to be considered. For instance, biochar particles can act as vapor-cracking catalyst and as long as the condensable vapors are in contact with biochar particles the effect of catalytic pyrolysis is yet to be considered. Therefore, the effect of catalytic particles by considering their unique chemical kinetics for secondary cracking can be a topic for future studies.

- **Effect of particle shrinkage:** in this paper the particles' size are considered uniform whereas the particle shrinks during the process. The effect of particle shrinkage can be taken into account by applying UDF to the models.

- **Moisture content and impurities in biomass feedstock:** this paper considers merely the lignocellulosic biomass whereas real biomass feedstock may contain moisture content and impurities. Therefore, considering these additional components necessitates some modifications for proposed chemical kinetics used for lignocellulosic biomass.

# 5. Conclusion

In this study, a CFD model is implemented for simulation of a fast pyrolysis process in a standard 2-D lab-scale bubbling fluidized bed. Euler-Euler approach with a multi-fluid model (MFM) for a gas phase and two solid phases including multiple species involved in each phase are studied in the simulations. The multi-step global reaction mechanisms are considered to implement the chemical reactions.

The model validation is performed using experimental data for red oak fast pyrolysis. The predicted results for biochar are in good agreement with the experimental data. The results obtained for condensable vapours are comparable to the experimental ones. However, the results for non-condensable gases under predicted the experimental values.

The effect of various materials' properties and operating conditions on the product yield is also investigated. It is observed that operating temperature, both sidewall and nitrogen temperature, plays an important role in the yield optimization of product. The optimum temperature for production of bio-oil is in the range of 500-525°C. At higher temperatures and longer residence time, a large proportion of condensable vapours converts to non-condensable gases. Hence, using higher nitrogen velocity, and moving the biomass injector to a higher elevation up to the height of sand packing limit leads to higher condensable and lower non-condensable yields. When using larger biomass particle size, due to the effect of intraparticle temperature gradient the supplied heat is not sufficient to reach the centre of the particles and consequently unreacted biomass increases. When the product yield is divided into the reacted biomass parts, the same proportions (66, 20, and 14 % for condensable, non-condensable, and biochar, respectively) are observed. When biomass feed rate increased beyond 1.3 kg/h, the supplied heat for the effective reaction was not sufficient and consequently, the product yields decreased. Larger sand particles necessitate using higher carrier gas velocity for effective fluidization. Therefore, the obtained results for this parameter are similar to increasing effects of nitrogen velocity which has a shorter residence time which in turn means higher condensable and lower non-condensable. Preheating the virgin biomass as much as a net heat power of 6.52 watts resulted in 7.5 % more bio-oil yields whereas other products' yields remain constant. The model can also be used for any lignocellulosic biomass to see the effect of biomass component on product yields. It is predicted that the sum of cellulose and hemicellulose content of the material is a more favourable component for bio-oil production whereas the lignin content contributes to higher biochar yields.

# 6. References

[1] Blin J, Volle G, Girard P, Bridgwater T, Meier D. Biodegradability of biomass pyrolysis oils: Comparison to conventional petroleum fuels and alternatives fuels in current use. Fuel 2007;86:2679-86.

[2] Bhattacharya BC, Kumar S. Renewable energy in Asia: a technology and policy review. In: Proceedings of world renewable energy congress VI, Brighton; July 1–7, 2000.

[3] Tsai WT, Lee MK, Chang YM. Fast pyrolysis of rice husk: product yields and compositions. Bioresource Technology 2007;98:22–8.

[4] Klass DL. Waste Biomass Abundance Energy Potential and Availability. In: Biomass for renewable energy, fuels, and chemicals. Academic press 1998, p. 137-58.

[5] McKendry P. Energy production from biomass (part 1): overview of biomass. Bioresource technology 2002;83:37-46.

[6] Panwar NL, Rathore NS. Potential of surplus biomass gasifier based power generation: A case study of an Indian state Rajasthan. Mitigation and adaptation strategies for global change 2009;14:711-20.

[7] Tsai WT, Lee MK, Chang YM. Fast pyrolysis of rice straw, sugarcane bagasse and coconut shell in an induction-heating reactor. Journal of Analytical and Applied Pyrolysis 2006;76:230-7.

[8] Kim S-S, Kim J, ParkY-H, Park Y-K. Pyrolysis kinetics and decomposition characteristics of pine trees. Bioresource technology 2010;101:9797-802.

[9] Qi Z, Jie C, Tiejun W, Ying X. Review of biomass pyrolysis oil properties and upgrading research. Energy Conversion and Management 2007;48:87-92.

[10] Panwar NL, Kothari R, Tyagi VV. Thermo chemical conversion of biomass–Eco friendly energy routes. Renewable and Sustainable Energy Reviews 2012;16:1801-16.

[11] Hoogwijk M, Faaij A., Broek RVD, Berndes G, Gielen D. Turkenburg W, Exploration of the ranges of the global potential of biomass for energy. Biomass and bioenergy 2003; 25:119-33.

[12] Özbay N, Pütün AE, Pütün E. Structural analysis of bio-oils from pyrolysis and steam pyrolysis of cottonseed cake. Journal of Analytical and Applied Pyrolysis 2001;60:89-101.

[13] Goyal HB, Seal D, Saxena RC. Bio-fuels from thermochemical conversion of renewable resources: a review. Renewable and sustainable energy reviews 2008;12:504-17.

[14] Balat M, Balat M, Kırtay E, Balat H. Main routes for the thermo-conversion of biomass into fuels and chemicals. Part 1: Pyrolysis systems. Energy Conversion and Management 2009;50: 3147-57.

[15] Pütün AE, Özcan A, Pütün E. Pyrolysis of hazelnut shells in a fixed-bed tubular reactor: yields and structural analysis of bio-oil. Journal of Analytical and Applied Pyrolysis 1999;52:33-49.

[16] DEMİRBAŞ A. Hydrocarbons from pyrolysis and hydrolysis processes of biomass. Energy sources 2003; 25:67-75.

[17] Şensöz S, Can M. Pyrolysis of pine (Pinus brutia Ten.) chips: 1. Effect of pyrolysis temperature and heating rate on the product yields. Energy Sources 2002;24:347-55.

[18] Anca-Couce A, Sommersacher P, Scharler R. Online experiments and modelling with a detailed reaction scheme of single particle biomass pyrolysis; Journal of Analytical and Applied Pyrolysis 2017;127:411-25.

[19] Rezaei H, S. Sokhansanj S, Lim CJ. Minimum fluidization velocity of ground chip and ground pellet particles of woody biomass. Chemical Engineering and Processing-Process Intensification 2017;124:222-34.

[20] Guizani C, Valin S, Billaud J, Peyrot M, Salvador S. Biomass fast pyrolysis in a drop tube reactor for bio oil production: Experiments and modeling. Fuel 2017;207:71-84.

[21] Shen J, Wang X-S, Garcia-Perez M, Mourant D, Rhodes MJ, Li CZ. Effects of particle size on the fast pyrolysis of oil mallee woody biomass Fuel 2009:88:1810-7.

[22] Westerhof RJM, Kuipers NJM, Kersten SRA, van Swaaij WPM, Controlling the water content of biomass fast pyrolysis oil. Industrial & Engineering Chemistry Research 2007;46:9238-47.

[23] Septien S, Valin S, Dupont C, Peyrot M, Salvador S. Effect of particle size and temperature on woody biomass fast pyrolysis at high temperature (1000–1400 C). Fuel 2012;97:202-10.

[24] Liu B, Papadikis K, Gu S, Fidalgo B, Longhurst P, Li Z, Kolios A. CFD modelling of particle shrinkage in a fluidized bed for biomass fast pyrolysis with quadrature method of moment. Fuel Processing Technology 2017;164:51-68.

[25] Cardoso J, Silva V, Eusébio D, Brito P, Tarelho L. Improved numerical approaches to predict hydrodynamics in a pilot-scale bubbling fluidized bed biomass reactor: A numerical study with experimental validation. Energy Conversion and Management 2018;156:53-67.

[26] Xiong Q, Kong S-C, Modeling effects of interphase transport coefficients on biomass pyrolysis in fluidized beds. Powder Technology 2014;262:96-105.

[27] Xiong Q, Zhang J, Xu F, Wiggins G, Daw CS. Coupling DAEM and CFD for simulating biomass fast pyrolysis in fluidized beds. Journal of Analytical and Applied Pyrolysis 2016;117:176-81.

[28] Ranganathan P, Gu S. Computational fluid dynamics modelling of biomass fast pyrolysis in fluidised bed reactors, focusing different kinetic schemes. Bioresource technology 2016;213:333-41.

[29] Xiong Q, Aramideh S, Passalacqua A, Kong S-C. BIOTC: an open-source CFD code for simulating biomass fast pyrolysis. Computer Physics Communications 2014;185:1739-46.

[30] Xiong Q, Aramideh S, Kong S-C. Assessment of devolatilization schemes in predicting product yields of biomass fast pyrolysis. Environmental Progress & Sustainable Energy 2014;33:756-61.

[31] Mellin P, Kantarelis E, Yang W. Computational fluid dynamics modeling of biomass fast pyrolysis in a fluidized bed reactor, using a comprehensive chemistry scheme. Fuel 2014;117:704-15.

[32] Boateng AA, Mtui PL. CFD modeling of space-time evolution of fast pyrolysis products in a bench-scale fluidized-bed reactor. Applied Thermal Engineering 2012;33:190-8.

[33] Xue Q, Dalluge D, Heindel TJ, Fox RO, Brown RC. Experimental validation and CFD modeling study of biomass fast pyrolysis in fluidized-bed reactors. Fuel 2012;97:757-69.

[34] Mellin P, Zhang Q, Kantarelis E, Yang W. An Euler–Euler approach to modeling biomass fast pyrolysis in fluidized-bed reactors–Focusing on the gas phase. Applied Thermal Engineering 2013;58:344-53.

[35] Xiong Q, Aramideh S, Kong S-C. Modeling effects of operating conditions on biomass fast pyrolysis in bubbling fluidized bed reactors. Energy & Fuels 2013;27:5948-56.

[36] Papari S, Hawboldt KA. A review on the pyrolysis of woody biomass to bio-oil: Focus on kinetic models, Renewable and Sustainable Energy Reviews 2015;52:1580-95.

[37] Xue Q, Heindel TJ, Fox RO. A CFD model for biomass fast pyrolysis in fluidized-bed reactors. Chemical Engineering Science 2011;66:2440-52.

[38] Xiong Q, Kong S-C, Passalacqua A. Development of a generalized numerical framework for simulating biomass fast pyrolysis in fluidized-bed reactors. Chemical Engineering Science 2013;99:305-313.

[39] Trendewicz A, Braun R, Dutta A, Ziegler J. One dimensional steady-state circulating fluidized-bed reactor model for biomass fast pyrolysis. Fuel 2014;133:253-62.

[40] Blanco A, Chejne F. Modeling and simulation of biomass fast pyrolysis in a fluidized bed reactor. Journal of Analytical and Applied Pyrolysis 2016;118:105-14.

[41] Hejazi B, Grace JR, Bi X, Mahecha-Botero A, Coupled reactor and particle model of biomass drying and pyrolysis in a bubbling fluidized bed reactor. Journal of Analytical and Applied Pyrolysis 2016;121:213-29.

[42] Papari S, Hawboldt KA, Helleur R. Production and Characterization of Pyrolysis Oil from Sawmill Residues in an Auger Reactor. Industrial & Engineering Chemistry Research 2017;31:10833-41.

[43] Jalalifar S, Ghiji MM, Abbassi R, Garaniya V, Hawboldt KA, Numerical modelling of a fast pyrolysis process in a bubbling fluidized bed reactor. In: IOP Conference Series: Earth and Environmental Science 2017;73:012032.

[44] Eri Q, Wang B, Peng J, Zhao X, Li T, Detailed CFD modelling of fast pyrolysis of different biomass types in fluidized bed reactors. The Canadian Journal of Chemical Engineering 2018;9999:1-10.

[45] Kulkarni SR, Vandewalle LA, Gonzalez-Quiroga A, Perreault P, Heynderickx GJ, Van Geem KM, et al. CFD-assisted Process Intensification Study for Biomass Fast Pyrolysis in a Gas-Solid Vortex Reactor. Energy & Fuels 2018 [just accepted].

[46] Peng J, Eri Q, Zhao X. Detailed simulations of fast pyrolysis of biomass in a fluidized bed reactor. Journal of Renewable and Sustainable Energy 2018;10:013104.

[47] Zhong H, Zhang J, Zhu Y, Liang S. Multi-fluid modeling biomass fast pryolysis with particle shrinkage model for complex reaction kinetics. Chemical Engineering and Processing-Process Intensification 2018;128: 36-45.

[48] Lathouwers D, Bellan J, Modeling of dense gas–solid reactive mixtures applied to biomass pyrolysis in a fluidized bed, International Journal of Multiphase Flow 2001;27;2155-87.

[49] Lathouwers D, Bellan J. Yield optimization and scaling of fluidized beds for tar production from biomass. Energy & Fuels 2001;15:1247-62.

[50] Aramideh S, Xiong Q, Kong S-C., Brown RC. Numerical simulation of biomass fast pyrolysis in an auger reactor. Fuel 2015;156:234-42.

[51] Xiong Q, Aramideh S, Passalacqua A, Kong S-C. Characterizing effects of the shape of screw conveyors in gas–solid fluidized beds using advanced numerical models. Journal of Heat Transfer 2015;137:061008.

[52] Rodriguez-Alejandro DA, Zaleta-Aguilar A, Rangel-Hernández VH, Olivares-Arriaga A. Numerical simulation of a pilot-scale reactor under different operating modes: Combustion, gasification and pyrolysis. Biomass and Bioenergy 2018;116:80-8.

[53] Yu X, Blanco PH, Makkawi Y, Bridgwater AV. CFD and experimental studies on a circulating fluidised bed reactor for biomass gasification, Chemical Engineering and Processing-Process Intensification 2018;130:284-95.

[54] Eri Q, Peng J, Zhao X. CFD simulation of biomass steam gasification in a fluidized bed based on a multi-composition multi-step kinetic model. Applied Thermal Engineering 2018;129:1358-68.

[55] Abboud AW, Guillen DP. Sensitivity study of a full-scale industrial spray-injected fluidized bed reactor. Powder Technology 2018;334:36-52.

[56] Brandão FL, Verissimo GL, Leite MAH, Leiroz AJK, Cruz ME. Computational study of sugarcane bagasse pyrolysis modeling in a bubbling fluidized bed reactor. Energy & Fuels 2018;32:1711-23.

[57] Cordiner S, Manni A, Mulone V, Rocco V. Biomass pyrolysis modeling of systems at laboratory scale with experimental validation. International Journal of Numerical Methods for Heat & Fluid Flow 2018;28:413-38.

[58] Xiong Q, Xu F, Ramirez E, Pannala S, Daw CS. Modeling the impact of bubbling bed hydrodynamics on tar yield and its fluctuations during biomass fast pyrolysis. Fuel 2016;164:11-7.

[59] Upadhyay M, Park HC, Choi HS. Multiphase fluid dynamics coupled fast pyrolysis of biomass in a rectangular bubbling fluidized bed reactor: Process intensification, Chemical Engineering and Processing:Process Intensification 2018;128:180-7.

[60] Gidaspow D. Multiphase flow and fluidization: continuum and kinetic theory descriptions, Academic press 1994.

[61] Demirbaş A. Mechanisms of liquefaction and pyrolysis reactions of biomass. Energy conversion and management 2000;41:633-46.

[62] de Velden MV, Baeyens J, Brems A, Janssens B, Dewil R. Fundamentals, kinetics and endothermicity of the biomass pyrolysis reaction. Renewable energy 2010;35:232-42.

[63] Shafizadeh F, Chin PPS. Thermal deterioration of wood. In: ACS Publications 1977.

[64] Han J, Kim H. The reduction and control technology of tar during biomass gasification/pyrolysis: an overview. Renewable and Sustainable Energy Reviews 2008;12:397-416.

[65] Authier O, Ferrer M, Khalfi A-E, Lédé J. Solid Pyrolysis Modelling by a Lagrangian and Dimensionless Approach--Application to Cellulose Fast Pyrolysis. International Journal of Chemical Reactor Engineering 2010;8:A78

[66] Yang H, Yan R, Chen H, Zheng C, Lee DH, Liang DT. In-depth investigation of biomass pyrolysis based on three major components: hemicellulose, cellulose and lignin. Energy & Fuels 2006;20:388-93.

[67] Ward SM, Braslaw J. Experimental weight loss kinetics of wood pyrolysis under vacuum. Combustion and flame 1985;61:261-9.

[68] Koufopanos CA, Lucchesi A, Maschio G. Kinetic modelling of the pyrolysis of biomass and biomass components. The Canadian Journal of Chemical Engineering 1989;67:75-84.

[69] Koufopanos CA, Papayannakos N, Maschio G, Lucchesi A. Modelling of the pyrolysis of biomass particles. Studies on kinetics, thermal and heat transfer effects. The Canadian journal of chemical engineering 1991;69:907-15.

[70] Orfao JJ, Antunes FJA, Figueiredo JL. Pyrolysis kinetics of lignocellulosic materials—three independent reactions model. Fuel 1999;78:349-58.

[71] Miller RS, Bellan J. A generalized biomass pyrolysis model based on superimposed cellulose, hemicelluloseand liqnin kinetics. Combustion science and technology 1997;126:97-137.

[72] Xiong Q, Yang Y, Xu F, Pan Y, Zhang J, Hong K, et al. Overview of Computational Fluid Dynamics Simulation of Reactor-Scale Biomass Pyrolysis. ACS Sustainable Chemistry & Engineering 2017;5:2783-98.

[73] Matta J, Bronson B, Gogolek PEG, Mazerolle D, Thibault J, Mehrani P. Comparison of multi-component kinetic relations on bubbling fluidized-bed woody biomass fast pyrolysis reactor model performance. Fuel 2016;210:625-38.

[74] Ranzi E, Cuoci A, Faravelli T, Frassoldati A, Migliavacca G, Pierucci S, et al. Chemical kinetics of biomass pyrolysis. Energy & Fuels 2008;22:4292-300.